Combined Shock and Vibration Isolation Through the Self-Powered, Semi-Active Control of a Magnetorheological Damper in Parallel with an Air Spring

E. Troy Tanner

Dissertation submitted to the faculty of the Virginia Polytechnic Institute and State University in partial fulfillment of the requirements for the degree of

Doctor of Philosophy
in
Mechanical Engineering

Daniel J. Inman, Co-Chairman
Mehdi Ahmadian, Co-Chairman
Harry H. Robertshaw
Donald J. Leo
Douglas K. Lindner

November 7, 2003
Blacksburg, Virginia

Keywords: Shock Isolation, Vibration Isolation, Magnetorheological Damper

Combined Shock and Vibration Isolation Through the Self-Powered, Semi-Active Control of a Magnetorheological Damper in Parallel with an Air Spring

E. Troy Tanner

Abstract

Combining shock and vibration isolation into a single isolation system package is explored through the use of an air spring in parallel with a controlled magnetorheological fluid damper. The benefits of combining shock and vibration isolation into a single package is discussed. Modeling and control issues are investigated and test and simulation results are discussed. It is shown that this hybrid isolation system provides significantly increased performance over current state-of-the-art passive systems. Also explored is the feasibility of scavenging and storing ambient shipboard vibration energy for use in powering the isolation system.

To date the literature has not adequately explored the direct design of a combined shock and vibration isolation system. As shock and vibration isolation are typically conflicting goals, the traditional approach has been to design separate shock and vibration isolation systems and operate them in parallel. This approach invariably leads to compromises in terms of the performance of both systems. Additionally, while considerable research has been performed on magnetorheological fluids and devices based on these fluids, there has been little research performed on the use of these fluids in devices that are subjected to high velocities such as the velocity seen by a ship exposed to underwater near-miss explosive events. Also missing from the literature is any research involving the scavenging and storage of ambient shipboard vibration energy. While the focus of this work is on the use of this scavenged energy to power the subject isolation system, many other uses for this energy can be envisioned.

Experimental and analytical results from this research clearly show the advantages of this hybrid isolation system. Drop tests show that inputs as great as 167 g's were reduced to 3.42 g's above mount at 1.11 inches of deflection using a Velocity Feedback controller suggested by the author. When contrasted with typical test results with similar inputs, the subject isolation system achieved reductions in above mount accelerations of 300% and reductions in mount deflections of 200% over current state-of-the-art passive shipboard isolation systems. Furthermore, simulations using a validated model of the isolation system suggest that this performance improvement can be achieved in multi-degree-of-freedom isolation systems as well. It was shown that above mount accelerations in the vertical and athwartship directions could be effectively limited to a predefined value, while achieving the absolute minimum mount defections, using an Acceleration Limiting Bang-Bang controller suggested by the author. Further experimentation suggests that the subject isolation system could be entirely self-powered from scavenged ambient shipboard vibration energy. An experiment using an energy scavenging and storage system consisting of a Piezoelectric Stack Generator and a bank of ultracapacitors showed that enough energy could be harvested to power the isolation system though several shock events.

Dedication

I would like to dedicate this dissertation to my mother Marlene Tanner and my grandfather, Albert Ford. My mother taught me the value of hard work and to this day she is the hardest working person I know. During my younger years she struggled working several jobs to make sure that our family had what we needed. My grandfather taught me what it was to be a decent human being. He was the kindest, most virtuous man I have ever known and he would do anything for anyone in a time of need. I only hope that at the end of my life I can look back and say that my mother and grandfather would have been proud of me.

Acknowledgements

I would first like to thank my wife, Kelly, and kids, Riley, Braden and Collin, for putting up with my addiction to education which lead to my pursuit of this degree. They have had to make many sacrifices over the years while I have been working and going to school and I truly appreciate their support.

Special thanks are in order for my two co-advisors, Dr. Dan Inman and Dr. Mehdi Ahmadian. Drs. Inman and Ahmadian have shown great patience and support while dealing with the difficulties and frustrations of advising an off-campus student working in industry. I could not ask for a better pair to guide me through the overwhelming task of getting to this point in my studies. I would also like to thank Dr. Harry Robertshaw, Dr. Don Leo and Dr. Doug Lindner for serving on my committee. Furthermore, Drs. Robertshaw and Leo deserve a special thanks for teaching controls to an old guy with no controls background. Whoever said you can't teach an old dog new tricks?

I would also like to thank Bob Marshall, my Supervisor at Northrop Grumman Newport News, for all of his help in pushing my company to realize the potential, and ultimately funding, this research. Bob never gave up no matter how dim the prospects became. Bob was also very supportive of my pursuing an advanced degree and helped me considerably in working out the logistics of taking classes, exams, and trips to Virginia Tech by working around my schedule.

Finally I would like to thank Doug Huebner of Newport News for teaching me much of what I needed to know about electronics and the practical aspects of implementing control and data acquisition systems. Doug's knowledge of electronics and engineering in general is no less than amazing. There is not a single subject in engineering that Doug is not familiar with. I am convinced that if Doug had not chosen engineering as a career he would have made a great teacher.

Contents

List of Figures

List of Tables

Chapter 1

Introduction

1.1 Overview

A classic problem in isolation system design is the design of a single isolator that can perform equally well as both a shock and a vibration isolator. This problem arises due to the fact that a good vibration isolator tends to be a poor shock isolator and vice versa. Most attempts to solve the combined isolation problem with a passive device quickly lead to frustration. This is certainly the case in shipboard isolation applications where many different inputs are often present simultaneously. The typical approach to solving the shipboard isolation problem involves utilizing separate passive isolators for shock and vibration. This inevitably leads to modifying vibration isolators to survive shock inputs and/or modifying shock isolators to perform adequately as vibration isolators. Inevitably the result of using this approach is less than optimal isolation performance.

When combined shock and vibration isolation is a design goal a semi-active isolation system becomes attractive. Semi-active isolation systems can be designed to simultaneously isolate for the combined and varying inputs that are present in shipboard applications. The physical advantages to combining shock and vibration isolation into a single package are obvious. A single combined isolation system replaces at least two separate systems and therefore reduces weight and increases available volume. This is particularly important in submarine applications where space is limited. Furthermore, with varying and diverse inputs, a combined semi-active isolation system can be designed to perform better than separate passive shock and vibration isolation systems operating in parallel. With careful design procedures the result can be nearly mathematically optimal isolation performance.

For shipboard applications the ideal isolation system would provide effective acoustic, vibration, and shock isolation from a variety of inputs such as underwater explosions, wave slap, impact, etc. Thus a "soft" isolator with a natural frequency no greater than say 2 Hz is desired that can survive various shock inputs. An ideal vibration isolator that meets this design criteria is an air spring. Air springs have a low natural frequency and are excellent shock isolators during the initial shock transient. Unfortunately, they tend to behave poorly as shipboard shock isolators due to the fact that shock events, such as underwater explosions (UNDEX), tend to drive the air spring into resonance following the initial transient. An air spring, being an inherently low frequency and lightly damped device, tends to undergo large deflections at resonance. Clearly this is undesirable in shipboard applications due to ever present tight rattle space requirements.

An ideal combined isolator would be an air spring that could provide large, variable damping forces on demand during a shock event. Producing large, variable damping forces is an ideal application for a magnetorheological (MR) fluid damper. Therefore, combining an air spring with a parallel-mounted MR damper would provide an ideal combined isolation system provided the damping force can be applied and varied rapidly enough to attenuate the shock input and simultaneously meet rattle space requirements.

A further motivation for investigating the MR damper as an isolator element is the current desire to introduce Commercial Off-the-Shelf (COTS) equipment into the shipboard environment. COTS equipment is typically categorized as either Industrialized COTS equipment or Commercial-Grade COTS equipment. Industrialized COTS equipment typically requires a 15g maximum above mount environment and Commercial-Grade COTS equipment typically requires a 7 to 8g maximum above mount environment. Furthermore, it is anticipated that in the near future COTS equipment manufacturers will be seeking to achieve above mount environments as low as 5 g’s. These environments are very difficult to achieve with passive isolators, particularly if stringent vibration isolation specifications need also be met simultaneously. However,

numerical studies and experimental data have shown that both shock and vibration specifications for all grades of COTS equipment can be easily met by using an isolation system consisting of an MR damper in parallel with an air spring. Furthermore, with current refresh rates for electronic equipment now approaching 18 months, the weight of the equipment, and its center-of-gravity is very likely to change with each refresh. Therefore, a re-evaluation and/or replacement of the isolation system could conceivably be required every 18 months. This is a very costly and time-consuming process. A semi-active isolation system can be designed to automatically adapt to variations in equipment mass and center-of-gravity as new equipment is introduced.

One drawback to any semi-active system is the need for a power source, with its associated cabling, as well as additional cabling to connect to an external controller. This problem is recognized and has stalled many attempts to use semi-active devices in shipboard isolation systems. MR devices are attractive in that they have low power requirements, are inherently stable, and in the absence of power they still behave as passive dampers. The later is particularly attractive as a failsafe feature as there is no guarantee that power will be available to the isolation system during battle conditions. A benefit of having low power requirements is that it may be possible to create a self-powered device. This could conceivably be accomplished by scavenging vibration energy and storing it to drive the MR damper/control system during a shock event. Having a self-powered, self-contained, combined shock and vibration isolator would be especially attractive as it would eliminate the need for external power sources and external controller connections.

1.2 Research Approach

The following outlines the approach taken for this research effort. First a simple single degree-of-freedom (SDOF) model of the isolation system was developed. This allowed a survey of control methodologies to be performed by simulation of the algorithms that have been successfully implemented in the past for controlling the MR

damper. This was done to determine the optimum control algorithm for use with ship shock inputs from the currently accepted control algorithms for the MR damper. The results of the simulations suggested that Linear Quadratic Regulator (LQR) optimal control provided the best performance of the algorithms tested. LQR was then used as an example for comparison for the other controllers that were developed. In an attempt to minimize the number of sensors required to implement LQR a controller was developed that utilized velocity feedback. This controller was designed to provide an energy loss per cycle that was as close as possible to being equivalent to that obtained with LQR control. This approach was driven by the nature of a ship-shock input due to an underwater near-miss explosion. These events tend to be fairly low cycle thus the maximum energy loss per cycle is desired in a ship-shock isolation system.

The LQR and velocity feedback controllers were then tested experimentally in a custom designed drop test machine. The design of the drop test machine was part of this effort. The drop test subjected the isolation system to a true base excitation shock event that was similar in acceleration magnitude to that seen in a Floating Shock Platform (FSP) test which is a standard Navy test platform. The FSP is essentially a barge to which can be fitted deck simulators of varying frequencies. The excitation is provided by underwater high-explosive charges at various stand-off distances. The test data suggested that the isolation system was very effective at isolating some very significant shock inputs with both of the control algorithms. The test data was also used to validate the single degree-of-freedom model. Very good correlation was achieved between the test and simulation data.

In an attempt to determine whether it would be feasible to power the isolation system using scavenged ambient shipboard vibration energy, the energy requirements for powering the device through a single shock event was determined. While in a practical application it would be desirable to be able to power the system through several shock events, for this test the design goal was set for powering the isolation system through one event. This was done with the realization that the approach could be scaled up to scavenge and store more energy fairly easily. For this study it was assumed that the

energy to be scavenged would come from a vibrating deck. Therefore, it was necessary to determine the amplitude and frequency of the available driving force. This was done analytically and verified through simulation. A survey of candidate power scavenging devices was then conducted and it was determined that a Piezoelectric Stack Generator (PSG) appeared to be an ideal device for the small amplitude, relatively high force inputs available to drive the device. Although several means exist for storing the scavenged energy, a stack of ultracapacitors was selected for this test. The PSG and the ultracapacitor stack was then tested experimentally both separately and as a system. Comparison was made with the expected performance from simulation and reasonable agreement was achieved.

From insight into the ship shock problem another controller was developed that limited the above mount acceleration to a preset maximum. Simulation suggested that this controller was ideal for use in ship shock applications as it simultaneously limited the above mount acceleration while minimizing the mount deflection. The later is desirable as ships typically have very tight rattle space requirements.

Using the validated SDOF model a three degree-of-freedom (3DOF) model of a generic equipment cabinet isolated with the subject isolation system was developed. In shipboard applications a 3DOF model is of sufficient fidelity to determine the response of an isolated piece of equipment since the vast majority of the input energy occurs in the vertical and athwartship (port-starboard) directions. Very little energy is input in the fore-aft direction. This model allowed an examination of the isolation system performance due to simultaneous multi-axis inputs and included the effects of rotation of the isolated equipment. The simulation results with the 3DOF model suggested that the acceleration limiting controller was very effective in simultaneously limiting above mount acceleration in both axes, as well as minimizing mount deflections and cabinet rotation.

Chapter 2

Literature Review

2.1 Overview

A comprehensive review of the available literature was conducted to determine the uniqueness of the subject areas of research. The specific areas of interest that were investigated were: (1) magnetorheological or electrorheological fluid devices and their applications, (2) the design of isolation systems that are specifically designed for combined shock and vibration isolation, (3) active and semiactive mounts, (4) self-powered isolation systems, and (5) the scavenging of ambient energy. The following approach was taken to complete the search. First an internet search was performed to find any available papers that were accessible via the internet or included contact information. The papers were then downloaded form the internet or the author was contacted to obtain a copy of the paper. The initial papers obtained, as well as the reference list from each of these papers, was then used to compile a master reference list. Next a search on the above topics was conducted using the ISI Web of Science service. All of the hits using this approach were added to the master list. Finally any contacts familiar to the author that happened to be working in this general area of research were contacted in an effort to obtain any papers they may have published. All of these papers were compiled in the master list.

The original master list contained 274 papers. At this point it became clear that the resources necessary to retrieve the remaining papers was beyond the capabilities of those available to the author. Thankfully, Dr. Inman offered to have an on-campus student track down as many of the papers on the master list as possible. Approximately half of the papers could not be found due to their age or the cost of obtaining a copy. The papers that were retrieved were further culled by eliminating any papers whose topics

were not similar to the subject work. The result was a compilation of 91 papers whose content is summarized in the next sections.

2.2 Magnetorheological or Electrorheological Fluids and their Applications

For the purpose of this review, magnetorheological and electrorheological fluids were lumped together due to the similarity in their mechanical properties. Any paper that discussed MR and/or ER fluids was considered acceptable for review. The MR and ER fluid papers were separated into the following sub-topics.

2.2.1 Fluid Properties and Modeling

Many of the papers whose topics involved MR and ER fluids were concerned with the mechanical properties of the fluids and/or modeling of these properties. 28 of the papers reviewed were devoted to the discussion or modeling of the properties of these unique fluids. The following is a review of the literature that explored MR or ER fluid properties and their modeling.

Ashour, Rogers and Kordonsky [1] discussed the basic properties of MR fluids and their potential applications in vibration control problems. The complete process from the manufacture of the fluid to its application in a cross stepper exercise machine was discussed. The manufacture of the fluid in a high-speed bead mill was shown to produce a high quality MR fluid. The characterization of the resulting fluid was discussed and the increase of the apparent viscosity with the magnetic field strength was shown to be as high as two orders of magnitude with moderate magnetic fields. The importance of the MR throttle valve in MR devices was discussed and it was shown that the greatest increase in apparent viscosity occurs when the flow direction of the MR fluid is normal to

the magnetic field direction. As an application example, a conventional damper in a commercial cross stepper exercise machine was retrofitted with an external throttle valve and the hydraulic fluid was replaced with MR fluid. It was shown that the resistance of the stroke of the foot pedals could be easily adjusted by varying the current to the coil in the throttle valve. Bossis, Lemaire, Volkova and Clercx [2] looked at two models for predicting the yield stress in MR and ER fluids.

Carlson, Catanzarite, and St. Clair [3] discussed the history of ER and MR fluids mentioning that the first paper on ER fluids was published in 1949 and the first patent was issued in 1947, both to Willis M. Winslow. Also mentioned was that the first papers on MR fluids were written in 1948 and the first patent was issued in 1951, both to Jacob Rabinow of the U.S. National Bureau of Standards. Several advantages of MR fluids over ER fluids were pointed out. The two basic modes of operation for MR devices were shown to be fixed poles (valve mode) or relatively moving poles (direct-shear mode). It was further shown that to achieve comparable performance an ER fluid device requires an active fluid volume that is 100-1000 times as large as that of an MR device. However, it was shown that both devices would have similar power requirements, the problem being that ER devices require high voltage at low current while MR devices require higher current at low voltage. Three examples of commercially available MR fluid devices were discussed: A MR Fluid Linear Damper for use in vehicle seat suspensions, a MR Fluid Rotary Brake for use in aerobic exercise equipment, and an MR Fluid Vibration Damper that can be used as a controllable dashpot.

Chang and Roschke [4] explored the development of a multi-layer perceptron neural network model for the MR damper. It was shown that the model satisfactorily represented dynamic behavior of the MR damper and therefore represents an adequate alternative to the typical characterization models that consist of a system of non-linear differential equations. Chu, Lee, and Ahn [5] explored the effect of changes in squeeze flow behavior of ER fluids as applied electric field, volume concentration of silica particles, viscosity of the carrier medium and water content in the silica was varied.

Felt, Hagenbuchle, Liu and Richard [6] investigated the rheological behavior of an MR fluid. It was shown that exposure of MR fluids to a magnetic field eventually leads to non-Newtonian rheology, i.e., the occurrence of yield stress and shear thinning. The dependence of apparent viscosity of the fluids on shear rate, field strength, volume fraction of ferrous particles and diameter of the ferrous particles was explored. It was shown that the dynamic yield stress increases in proportion to both the volume fraction and particle size of the ferrous particles. In addition, it was shown that the shear stress in the fluid is proportional to the square of the applied field. Furthermore, it was shown that the rheology of MR fluids is very similar to the rheology of ER fluids. It was suggested that the commonly used Bingham model gives an insufficient rheological description of the MR fluid as it does not account for the effect of shear thinning.

Gamota and Filisko [7] explored the response of an ER fluid consisting of alumino-silicate particles in paraffin oil to sinusoidally oscillating shear strains ranging in frequency from 10 to 50 Hz. It was shown that the response of the fluid can be divided into three distinct regions; pre-yield, yield and post-yield. Furthermore, it was shown that the material behaves as a viscoelastic material in the pre-yield region, a viscoelastic-plastic material in the yield region, and a plastic material in the post-yield region. These modes are dependent on the applied electric field strength, strain amplitude and strain frequency. It was determined that the energy dissipated by the ER material is proportional to the strain raised to the second power in the pre-yield region, varies between the strain raised to the second power and raised to the first power in the yield region, and is proportional to the strain in the post yield region. A model for the ER material was proposed consisting of a Zener element in series with a Coulomb and a viscous element that describes the general behavior of the material as it changes from viscoelastic to viscoeleastic-plastic. It was shown that as the electric field increased both the ER fluid's viscous and elastic components increase. Thus, the material has increased its energy dissipating and energy absorbing capability.

Gorodkin, Lukianovich and Kordonski [8] investigated the modeling of the pressure-flowrate characteristics of an MR throttle valve in which the hydraulic

resistance characteristics of the valve are determined as a function of the Reynolds and Hedstrom numbers. It was shown that the hydraulic characteristics of the valve predicted by the Hedstrom technique accurately describes the characteristics of the valve. This was validated by comparison to experimental data. A procedure for prediction of the valve parameters necessary for damper design was suggested.

Jolly, Carlson and Munoz [9] explored the development of a quasi-static, one-dimensional model that accurately described the mechanical and magnetic properties of MR fluids and elastomers. The model needed to be fit to experimental magnetic induction curves by adjusting a parameter that accounts for the un-modeled magnetic interactions between neighboring particle chains. It was shown that these interactions decrease with decreasing particle volume fraction. Once fit to the experimental data the model was shown to be in relatively good agreement with published yield stress data for MR fluids as well as pre-yield data taken on MR elastomers.

Kamath and Wereley [10] discussed a nonlinear dynamic model that effectively described the electrorheological behavior of an ER fluid in terms of shear stress versus shear strain. The model combined a three-parameter fluid element and a viscous fluid element to accurately describe the shear flow behavior in the pre-yield and post-yield regimes, respectively. To accurately describe the behavior through the yield point a nonlinear combination of the linear shear flow mechanisms was utilized.

Kamath, Hurt and Wereley [11] discussed the development and validation of a model that described the rheological behavior of an ER damper. The model was based on an idealized nonlinear Bingham plastic shear flow mechanism. This mechanism predicts that in a typical annular valve three annular flow regions develop as a function of local shear stress. In the central region between the two electrodes, the so-called plug region, the local shear stress is less that the yield stress and the fluid behaves as a rigid solid. In the other two regions near the electrodes the local shear stress exceeds the yield stress and the material flows. It was shown that the damping behavior of an ER damper is strongly coupled with the behavior in the plug region. For a constant force, as the applied

field increases, the plug thickness and the equivalent viscous damping increase as well. For a constant applied field, as the force increases, the plug thickness and the equivalent viscous damping both decrease.

Kordonsky [12] discussed the modeling of an MR fluid valve (Here called a magnetorheological converter). The model takes into account the behavior of the magnetic field producing inductor. Also discussed is a concept for a MR actuator as well as the use of MR fluids as the working medium in seals.

Li, Chen, and Yeo [13] investigated the mechanical properties of MR fluids in the pre-yield region. The viscoelastic properties were measured with a parallel-plate strain-controlled rheometer. Two experiments were performed; a strain-amplitude sweep test and a frequency sweep test. The strain-amplitude sweep test varied the strain amplitude from 0.0001 to 0.001 at a fixed driving frequency of 10 Hz. The frequency sweep test varied the driving frequency from 1 Hz to 100 Hz at a constant strain amplitude of 0.001. The results showed that the both the storage modulus and the loss modulus increase with increasing frequency while both decrease with an increase in strain amplitude. It was also shown that an increase in magnetic field increases the storage modulus and loss modulus and an increase in volume fraction of ferrous particles leads to an increase in storage modulus.

Pang, Kamath and Wereley [14] discussed four models for describing the hysteresis behavior of a Lord Rheonetics SD-1000-2 MR damper. The four models discussed were: (1) nonlinear, Bingham plastic model, (2) nonlinear, biviscous model, (3) nonlinear, hysteretic biviscous model, and (4) nonlinear, viscoelastic-plastic model. It was shown that any of the models could predict the damper behavior adequately enough to estimate energy dissipation or damping. It was suggested that the nonlinear, viscoelastic-plastic model is superior to the other models for simulation because it is piecewise smooth in velocity. The other three models are only piecewise continuous in velocity. All of the models represent the force vs. displacement behavior of the damper equally well.

In the survey paper [15] Parthasarathy and Klingenberg discussed the current state of modeling of ER fluid behavior. Sims, Peel, Stanway, Johnson and Bullough [16] discussed the development of a model for an ER damper and its experimental verification. The model consisted of a spring, mass and a damper connected in series. The spring stiffness is based upon the bulk modulus of the ER fluid and the mass is determined from the fluid density. The damping characteristics were described by a non-dimensional, Bingham plastic function.

Sims, Stanway, Peel, Bullough and Johnson [17] discussed a control algorithm that effectively linearizes the response of an ER damper to mimic the response of a viscous damper using a proportional feedback control strategy. The result is the equivalent of a viscous damper with a continuously variable damping coefficient. It was shown experimentally that the slope of the force-velocity characteristics can be specified and modified through a change in a gain term in the controller. The effectiveness of the algorithm was shown at frequencies up to 5 Hz. Spencer, Dyke, Sain and Carlson [18] discussed the development and validation of the Modified Bouc-Wen model of the MR damper. The model was shown to accurately predict the force-displacement and force-velocity behavior of a Lord MR damper. A survey paper [19] by Stanway, Sproston and El-Wahed discussed the current (circa 1995) state of the use of ER fluids in vibration control.

Timko, Zentko, Zentkova, M., Koneracka, Kellnerova, Zentkova, A., Stepan and Barbora [20] discussed the effect of external magnetic field, velocity of flow and concentration of magnetic particles on the rheological properties of mineral oil-based MR fluids. It was shown that the apparent increase in the viscosity of the fluid increased with increasing external magnetic field and increasing concentration of ferrous particles. Furthermore, it was shown that at higher flow velocities the change of viscosity became smaller. It was suggested that this was due to breakup of the chain structure formed by the ferrous particles in the MR fluid.

Weiss, Carlson and Nixon [21] investigated the transition area between elastic and viscous behavior in ER and MR fluids. It was shown that the storage modulus for an MR fluid is several orders of magnitude greater than that of an ER fluid, and is in the range of common viscoelastic solids. Experiments showed that both MR and ER fluids yield at a strain level of less than 1%. It was suggested that this behavior may hinder the use of either fluid in applications that require stability in pre-yield properties. The authors felt that future R&D efforts should be focus on increasing the yield of these fluids to higher strain levels. In [22], Wereley and Pang discussed the nondimensional analysis of ER and MR dampers using approximate parallel plate models. However, the accuracy of the suggested models was not discussed.

2.2.2 Application to Control of Civil Structures

In terms of applications of MR and ER fluids, the vast majority of the published work has involved the use of these fluids in structural response control of civil structures. 31 of the papers reviewed were devoted to this topic. Of particular interest appears to be work involving earthquake hazard mitigation. Much of the civil structure work has been performed by Bill Spencer at Notre Dame and later by his former graduate student Shirley Dyke at the University of Washington.

Dyke and Spencer [23] investigated four different semiactive control algorithms for the MR damper. The algorithms considered were control based on Lyapunov stability theory, decentralized bang-bang control, modulated homogeneous friction and clipped optimal control. The clipped optimal controller is essentially a linear optimal controller that provides an optimal force value. A force feedback loop provides a measure of the actual damping force which is then compared to the optimal control force. Based on this comparison the voltage to the MR damper is varied to provide as near as possible the optimal control force. The force feedback loop uses readily available accelerometers as sensors. The performance of the various controllers was compared through the simulation of the response of a 3-story structure with an MR damper connected between

ground and the first story. The input for the simulations was the N-S component of the El Centro earthquake data. As a control, two additional cases were considered, one being a constant 0V being applied to the current driver and the other being a constant 2.25V being applied to the current driver. This corresponds to the minimum and maximum damping forces that can be generated by the MR damper. It was shown that all of the algorithms performed noticeably better than the passive controllers in some way. The largest reduction in the maximum acceleration was achieved with the decentralized bang-bang controller. The largest reduction in third floor displacement and peak interstory displacement was achieved with the clipped optimal controller. The paper also discusses the Modified Bouc-Wen model of the MR damper, although it is not mentioned by that name.

In [24], Dyke and Spencer continue the work of [23] by applying the clipped optimal control algorithm to a five-story structure. The paper also discusses the Modified Bouc-Wen model of the MR damper. In the experiment the dampers were placed between the first floor and ground as well as the first and second stories. It was shown that this damper placement using the clipped optimal control algorithm resulted in significant reductions in floor accelerations while simultaneously reducing interstory displacements. The inputs to the structure were data from the El Centro earthquake at three different magnitudes. The semiactive approach achieved a 22%, 28% and 32% reduction in the peak absolute acceleration over the best passive case while simultaneously achieving large reductions in the interstory displacements.

In [25], Dyke continued the studies begun in [23] and [24] and expands the simulation to the control of seismically excited 20-story building. The clipped optimal control algorithm is again employed to control a total of 30 dampers that were applied to control the structure. In addition to the dampers, the control system employed 36 sensors and the controller had 40 states. Four inputs were considered including the El Centro earthquake considered in the previous papers as well as the Hachinohe, Kobe and Northridge earthquakes. It was shown that the control system achieved significant reductions in all structural responses for all of the four earthquake excitations. Maximum

relative displacements were reduced by 21.6-55.8%, maximum normalized drift was reduced by 36.4-55.0%, maximum accelerations were reduced by 22.8-50.0% and base shear was reduced by 34.4-55.3% as compared to the uncontrolled values.

Dyke, Spencer, Quast, Kaspari and Sain [26] discussed the use of acceleration feedback control strategies based on H_2/LQG control design techniques to control the structural response of a three-story test structure using an active mass driver (AMD) mounted at the top of the structure. It was shown that under broadband excitation the AMD controller was able to achieve an 80% reduction in RMS acceleration responses as well as a significant response reduction in all three modes of the system. Furthermore, when excited by an earthquake disturbance, the reduction of the peak top floor acceleration was 65%.

In [27], Dyke, Spencer, Sain and Carlson extended the work performed in [26] which explored the effectiveness of the clipped optimal controller for controlling an MR damper mounted in a 3-story test structure. Two optimal controllers were considered. Controller A placed a heavy weighing on the third floor relative displacement. Controller B placed a heavy weighting on the third floor acceleration. As a control two passive cases were also considered. Passive off implied 0V was applied to the current driver of the MR dampers. Passive on implied 2.25V was applied to the current driver of the MR damper which corresponded to saturation of the magnetorheological effect. It was shown experimentally that when subjected to the N-S component of the El Centro earthquake Controller A achieved a 24.3% reduction in the peak third floor displacement and a 29.1% reduction in the maximum interstory displacement over the best passive case. Controller B achieved a 33.3% reduction in the peak third floor relative displacement over the best passive case although an increase in the maximum floor accelerations was also seen.

Dyke, Spencer, Sain and Carlson [28] explored the modified Bouc-Wen model of the MR damper as well as evaluated the performance of the MR damper and clipped optimal control algorithm for controlling the response of a scaled three-story building

model. It was shown that the performance of the semi-active clipped optimal controller surpassed that of an active controller while requiring a small fraction of the power. Dyke, Spencer, Sain, and Carlson [29] explored the efficiency of the MR damper in conjunction with the clipped optimal control algorithm to control the structural response of a scaled three-story structure. The structure was modeled and the model was validated. Three versions of the clipped optimal controller were utilized. Controller A placed a high weighting on the third-floor relative displacement. Controllers B and C placed low and high weighting, respectively, on the third floor acceleration. It was shown that the control system effectively reduced both the peak and RMS responses due to a broad class of seismic excitations over that of the response using both passive-off and passive-on control. All of the controllers achieved excellent results when compared to the passive cases. In addition, it was shown that the semi-active control systems were able to achieve these performance gains using smaller control forces than the passive-on case.

Dyke, Spencer, Sain and Carlson [30] discussed the modified Bouc-Wen model of the MR damper and its effectiveness at predicting the response of the MR damper. The paper then explored the effectiveness of the clipped optimal control algorithm in reducing the structural response of a scaled three-story structure model. It was shown that the clipped optimal control strategy performed better than either the passive-off or passive-on cases. Furthermore, the clipped optimal controller outperformed a simulated optimal active controller, while requiring only a small fraction of the power of the active system. In [31], Dyke, Spencer, Sain and Carlson present essentially the same information as in [30].

Dyke, Yi and Carlson [32] experimentally explore the effectiveness of utilizing shear mode MR dampers in conjunction with the clipped optimal control algorithm to control a six-story test structure. The control system employs four shear mode MR dampers which are claimed to produce a maximum force of 20kN (4500 lbf) each. It was shown that the semi-active controller is capable of surpassing the performance of the passive-on controller at the first two modes of vibration.

Housner, Bergman, Caighey, Chassiakos, Claus, Masri, Skelton, Soong, Spencer and Yao [33] present a survey paper that summarizes the current (circa 1997) state-of-the-art in structural control of civil engineering structures. The history of MR fluid devices is discussed from their discovery by Winslow (1947) to the current work by Spencer, Dyke and Carlson. The clipped optimal controller is mentioned briefly, but no technical information or performance characteristics are discussed.

Inaudi [34] discussed a control algorithm that makes the contact force between sliding surfaces of a friction damper proportional to the absolute value of the prior local peak of the damper displacement. This control logic results in a nonlinear force-displacement behavior such that when the damper displacement is scaled by a constant, the damper force is scaled by the same constant. The force-displacement hysteresis loops of the closed-loop system are rectangular and the area (energy dissipation) are proportional to the square of the damper displacement. This paper only discussed the modeling and control of a friction damper in a model of a six-story structure with the dampers installed as cross braces. No results that showed the effectiveness of the dampers with the proposed algorithm were discussed.

Jansen and Dyke [35] explored three nonlinear control algorithms: (1) control based on Lyapunov stability theory, (2) decentralized bang-bang control and (3) clipped optimal control. A modified Bouc-Wen model of the shear mode dampers that were utilized was developed. A numerical study of the response of a six-story structure controlled with four shear mode MR dampers controlled using the above algorithms was conducted. The test input was a scaled version of the N-S component of the El Centro earthquake. Two of the dampers were mounted between the first floor and ground and the other two were mounted between the first and second floors. Two versions of the Lyapunov and clipped optimal controllers were investigated (Denoted A and B), but it is not explained how these differ. As a control two passive controllers were also considered; Passive-off and passive-on. Based on the numerical results it was shown that all of the algorithms showed improvement over the best passive case. It was determined that two of the controllers were most suitable for use with multiple MR dampers, the

Lyapunov and clipped optimal controllers. The Lyapunov B controller was able to achieve the largest reduction in maximum floor displacement. The largest reduction in maximum interstory displacement and maximum absolute acceleration was achieved with the clipped optimal controller B and A, respectively.

In [36], Jansen and Dyke essentially expanded the work performed in [35] by adding the modulated homogeneous friction controller to the study. In addition, the differences between the Lyapunov and clipped optimal A and B controllers is explained. The two Lyapunov controllers have different Q_P matrices. The clipped optimal A controller placed a moderate weighting on the relative displacements of all floors. The clipped optimal B controller placed a higher weighing on the relative displacement of all floors. The results were as in [35] with the exception of the added modulated homogeneous friction controller which was shown to achieve a significant reduction in displacements and drifts at the expense of increased accelerations.

Makris, Burton and Taylor [37] discussed the design, analysis and modeling of an ER fluid damper developed for seismic response reduction in civil structures. A multi-layer neural network was developed and trained with an efficient algorithm known as the Dependence Identification Algorithm. It was shown that a neural network constructed with the Dependence Identification Algorithm and combined with a standard Maxwell model satisfactorily predicts the response of the damper with and without the presence of an electric field.

Makris, Burton, Hill and Jordan [38] discussed the mechanical behavior of a silicon oil based ER fluid and a damper that utilizes this fluid. The damper was designed for the reduction of seismic response and vibration in civil structures. The damper consisted of a cylinder and piston that pushed the ER fluid through an external annular duct. The electric field was applied to the fluid flowing through this duct. It was shown that the flow through the duct can be satisfactorily approximated with an elastic-viscoplastic model based on Hagen-Poiseille flow theory. Furthermore, it was shown that to have a significant contribution to the damper force from the ER effect, the flow rate

across the duct must be kept relatively small. It was suggested that this can be achieved by increasing the number of bypasses. This suggests that ER fluids may not be ideal for shock applications where high flow rates can be anticipated.

Masri, Kumar and Ehrgott [39] discussed the modeling and control of an ER damper for structural control applications. The model utilized was developed by fitting Chebyshev polynomials to experimental ER damper force data. It was shown that the damper model accurately predicts the damper behavior. The controller used appears to be based on optimal control, but sufficient detail is not presented to follow the control algorithm development. After determining an optimum damping force the controller uses a force-voltage function to determine the voltage to be applied to the damper. This controller was termed "pulse" control. It was suggested that the use of this controller produces a favorable reduction in displacement and acceleration response, but the one plot shown suggested only minimal performance improvement.

Quast, Sain, Spencer and Dyke [40] discussed digital control concepts and their application to the acceleration feedback control of a three-story test structure. The control force was provided by an active bracing system that utilized a hydraulic actuator. The controller was implemented on a Texas Instruments TMS320C30 DSP chip at a sampling rate of 1 kHz. Although the control strategy was not discussed in detail, it was shown experimentally that the digital controller reduced the absolute accelerations of the top two floors of the test structure by more than a factor of two.

Ramallo, Johnson and Spencer [41] discussed the use of sponge-type MR dampers in a base isolation system for the seismic control of structures. A modified clipped optimal control algorithm was used for control. When compared to the damper operating in an optimal passive mode (which was determined experimentally), the damper controlled with the modified clipped optimal control algorithm achieved significant accelerations reductions over the entire range of earthquake intensities considered.

Sadek and Mohraz [42] discussed three semi-active control algorithms for controlling variable dampers. The three algorithms discussed were: (1) Classic LQR control, (2) A modified LQR algorithm that places a penalty on the absolute acceleration of each DOF to place an additional emphasis on the structural accelerations, and (3) A semi-active displacement-acceleration domain algorithm that changes the damping coefficient based on the angle formed in the displacement-acceleration plane by the absolute acceleration and the displacement. It was shown that variable dampers are effective in reducing the responses in flexible structures, but not in rigid structures. The best performance in terms of displacement and acceleration response was achieved with the modified LQR algorithm. The other two algorithms achieved similar performance for SDOF structures, but the displacement-acceleration domain algorithm was not effective for MDOF structures.

Spencer and Sain [43] discussed the use of feedback control methods for the response control of civil structures. The paper reviews the control implementations that have already been incorporated in civil structures and discusses current research in the area of structural control. No results or mathematical description of algorithms are presented.

Spencer, Yang, Carlson and Sain [44] explored the development and validation of a model for a 20-ton MR damper designed for seismic protection of civil structures. The damper was designed and built by the Lord Corporation. Two models were considered; an axisymetric model and a simpler parallel-plate model. It was shown that the simpler parallel-plate model could accurately approximate the force-velocity behavior of the damper. It was also shown that the controllable force range is inversely related to the gap size.

In this survey paper [45] Symans and Constantinou compare passive, active, and semi-active structural control systems in a general sense. Also included is a review of the literature on semi-active structural control systems. Yang, Spencer, Carlson and Sain [46] discussed the modeling of the Lord 20-ton prototype MR damper using the modified

Bouc-Wen model. This damper was designed for full-scale implementation of MR dampers in civil structures. Excellent agreement was shown between the model and experimental data.

Yi and Dyke [47] explored the capabilities of ideal passive and active control systems on response reduction of structures. The passive system considered was an ideal passive damper. The ideal active system consisted of an ideal actuator using a H_2/LQG control algorithm. To evaluate the performance of the controllers, the structural response of 1, 3, 6, 10 and 20-story buildings was determined. In all cases the base excitation was white noise and the responses and control forces were recorded as RMS values. It was shown that active control offers no advantage over passive systems for the SDOF structure. However, as the number of degrees-of-freedom increased the performance of the active system surpassed that of the passive system and the performance increase was greater as the number of floors increased.

Yi, Dyke, Caicedo and Carlson [48, 49] discussed the results of a numerical study to determine the effectiveness of utilizing shear mode MR dampers in conjunction with the clipped optimal controller for seismic response reduction. This study used four randomly placed MR dampers in a six-story structure. Each damper was capable of producing 29 kN (6520 lb) of force. It was shown that this semi-active system achieved excellent performance, surpassing a number of optimal passive systems, while using a very small amount of power to do so. Yi, Dyke, Frech and Carlson [50] presented essentially the same material as in [48, 49].

Yoshida and Dyke [51] discussed a control solution to the third generation benchmark problem on structural control. This benchmark problem consisted of the control of a seismically-excited, full-scale, nonlinear, 20-story building. The control approach taken in this paper was the use of shear mode MR dampers that were controlled using the clipped optimal control algorithm as well as a modified clipped optimal control algorithm. The modified clipped optimal control algorithm assumed a linear relationship between the force produced by the damper and voltage applied to the current driver. It

was shown that both of the controllers provided performance that equaled, and in some cases exceeded, the performance of an active system. Furthermore, it was shown that the modified controller was significantly more effective at reducing structural accelerations, while achieving nearly the same reduction in interstory drifts, as with the non-modified controller.

2.2.3 Helicopter Lag Mode Damping

Marathe, Gandhi and Wang [52] investigated the use of a shear mode MR damper for improving lag damping in helicopter rotor blades. A model of the MR damper is incorporated into a mechanical model of the rotor. Two controllers were considered: An on-off controller and a feedback linearization controller. The on-off controller attempts to linearize the response of the nonlinear MR damper to approximate an equivalent linear damper. The feedback linearization controller attempts to linearize the force output of the nonlinear MR damper. It was shown that both controllers are effective in reducing ground resonance and reducing periodic damper loads in forward flight.

It should be noted that additional work in the area of helicopter lag mode damping has been performed by Norman Wereley at the University of Maryland, but none of Dr. Wereley's papers on this subject were readily available.

2.2.4 Automotive Applications

A sizable amount of MR fluid research has been performed for the automotive industry. However, due to the desire to protect proprietary material, it is difficult to find much literature on automotive applications of MR fluids available to the general public. What is clear is that MR damper-based suspension systems for automobiles have reached the production phase (Witness the MR damper-based suspensions on the new Cadillac

and Corvette). Reducing the cost of these systems will surely lead to their introductions on lower priced vehicles. Being very research oriented, the fact that the auto industry is paying this much attention to MR devices is a clear indication of the significant performance increases that can be obtained with these devices.

Carter's [53] thesis explores the transient response characteristics of a Class 8 truck using passive and semactive dampers. The response was simulated using a four-degree-of-freedom roll-plane model. Four different control policies were investigated including on-off skyhook, continuous skyhook, on-off groundhook and a newly developed method of fuzzy logic control. The results of the simulations show that compared to passive dampers, semiactive dampers have minimal effect on improving the vehicle body and tire transients due to forces or torques applied to the body. However, for road inputs the semiactive dampers are able to provide a more favorable compromise between the body and axle transient dynamics as compared to passive dampers. Furthermore, it was shown that the fuzzy logic semiactive control policy is better able to control body and axle dynamics than the more traditional semiactive policies that were investigated.

Choi and Cheong [54] discussed the development and testing of a suspension system consisting of an ER damper powered by a generator system consisting of a rack and pinion gear to transform the linear motion of the damper into rotary motion which was then amplified through additional gearing. The resulting rotary motion is then used to drive a generator and the energy is stored in a battery to power the damper and control circuitry. It was shown that this fairly complex system could generate enough power to operate the ER damper-based suspension. Furthermore, it was shown that acceptable vibration isolation could be achieved in terms of displacement transmissibility up to 2 Hz when utilized in a quarter car model.

McLellan [55] discussed the development and testing of a digital controller for a MR damper-based suspension system for a Class 8 truck. The controller used a skyhook policy to control the MR dampers which were installed in the truck's primary suspension

system. The controller utilized accelerometers that were placed on the truck's frame and axle. The completed control system was tested with both random (on highway) and impulse (speed bump) inputs. It was shown that the semiactively controlled MR dampers do not offer any significant benefits in reducing the overall vibration levels at the frame or axles. However, some benefit was realized with transient inputs (speed bumps).

Pare [56] discussed the development and testing of a semi-active suspension system for a passenger vehicle that utilized MR dampers. To test the system a full-scale, 2DOF, 1/4 car test apparatus was designed and built. Three control schemes were evaluated: (1) Skyhook control, (2) Groundhook control, and (3) Hybrid semiactive control (essentially combining both skyhook and groundhook control). Skyhook control was shown to be effective at isolating the motion of the sprung mass from the base excitation at the expense of excessive un-sprung mass motion. Groundhook control was shown to be effective at controlling the un-sprung mass motion at the expense of excessive sprung mass motion. Hybrid semiactive control (essentially a linear combination of skyhook and groundhook control) yielded a performance that essentially took advantage of the benefits of both skyhook and groundhook control. Finally, the MR dampers were installed in a Chevy Lumina in a constant voltage mode, i.e., the controllers were not utilized in the actual test vehicle.

Simon [57] discussed the design and testing of a MR damper-based, semi-active suspension system for a heavy truck. The dampers were controlled using a skyhook control policy. The performance was evaluated with two different inputs. The first was a transient input which was implemented by driving the truck over a speed bump at a relatively low (5-7 MPH) speed. The second was a random input which was achieved by driving the truck at 55 MPH on a straight and level highway. To determine the effective performance benefit of the MR damper-based suspension, the response was compared to the response with the stock suspension and passive-on and passive-off MR damper suspensions. For the transient input, it was shown that the MR damper-based suspension with the skyhook control policy showed a small change in vehicle body and wheel dynamics as compared to the stock suspension. However, in terms of peak accelerations

and displacements the MR suspension showed little performance improvement. For the random input the MR damper-based suspension achieved a significant improvement in performance over the stock suspension.

2.2.5 Gun Recoil Control Applications

The research on gun recoil control using MR dampers is the only work found that looked at using MR dampers in extremely high velocity applications. As such, this work represents the only work using MR dampers in systems that are subjected to the type of velocities that are seen in shipboard shock isolation applications.

Ahmadian and Poyner [58] discussed the application of MR dampers for controlling gun recoil dynamics. The development of a demonstrator consisting of a single-shot 50 caliber BMG rifle and a prototype MR damper was discussed. It was shown that the MR damper was very effective at reducing the recoil stroke of the gun at the expense of significantly increased recoil forces. This work, and that in [59], is significant in that it is the only known work on MR dampers subjected to very high velocities. In this effort no control was performed. A constant voltage was applied to the current drivers, which in turn supply the current to the dampers, and the resulting recoil stroke and force were measured for varying input voltages.

Ahmadian, Appleton and Norris [59] explored the application of MR dampers for controlling the dynamics of a fire out-of-battery (FOOB) recoil system for large guns using a dynamic simulation of a 105mm cannon. The FOOB system works by pre-accelerating the recoiling parts in the direction opposite to the recoil prior to ignition. It was shown through simulation that while conventional hydraulic recoil dampers can be designed and tuned to control FOOB as effectively as MR dampers, they cannot perform well when firing faults are encountered. The results showed that MR dampers were able to adapt to firing faults such as pre-fire, hang-fire and misfire and provided “soft-recoil”

under all firing conditions. Further work will apply this concept to actual hardware in the field.

2.2.6 Other Applications of MR/ER Fluid Devices

The following two papers did not fit into the categories established above for MR and ER-based device applications, but are still significant and are therefore included in this review.

Yalcintas and Dai [60] discussed the vibration control capabilities of MR and ER adaptive beam structures (essentially a beam constructed by sandwiching a layer of MR or ER fluid between two layers of a suitable substrate material). It was shown that both MR and ER materials were quite successful at controlling vibrations in adaptive beam structures.

Yao, Yap, Chen, Meng, Fang and Qiu [61] discussed the design and modeling of a multi-layer squeeze film ER damper and its application to the vibration control of a rotor system. It was shown that: (1) the damper can suppress large vibration amplitudes at the critical speed, (2) the on/off type control discussed successfully suppressed the resonance without causing rotor instability, (3) the damper can suppress sudden imbalance response, shorten the transient response and reduce the steady-state vibration amplitude, and (4) the suggested damper model accurately predicted the steady-state response and the sudden imbalance response.

2.3 Combined Shock and Vibration Isolation

No papers were found that specifically addressed the design of an isolation system for simultaneous isolation of shock and vibration. This was surprising as the design of an

isolation system that can perform adequately with both shock and vibration inputs is a significant problem

2.4 Self-Powered Isolation Systems

Nakano, et al., [62,63,64] developed a self-powered active vibration control system consisting of an energy regenerative damper (DC linear motor) that was used to generate energy which was then stored in a capacitor. The stored energy was then used to power another DC linear motor which was used as an actuator to provide active vibration control. This system was designed for use in isolating heavy truck cabs from road inputs. It was shown that the isolation system provided better performance than passive and semi-active isolation systems considered. These three papers were significant in that they were the only papers, other than that by Choi and Cheong [54] discussed above, that considered scavenging vibration energy to power an isolation system.

2.5 Active and Semiactive Mounts

The papers in this section discussed active and semiactive mount technologies that did not fit into any of the categories previously discussed, but whose subject was relevant to this discussion.

Ahmadian, Miller, Southward and Roemer [65] explored the development and performance of a prototype active mount for commercial jet isolation application. The mount consisted of a prototype fluid mount which was originally developed for aircraft engine mount applications that had been retrofitted with an electromagnetic actuator to control fluid flow and thus mount force actively. The controller was based on an adaptive Least Mean Square (LMS) algorithm and was implemented digitally on a DSP.

The isolated structure consisted of two beams of different resonant frequencies to which were attached two accelerometers. The accelerometers provided the feedback signals for the control algorithm. For test purposes the below mount excitation was provided by an MTS load frame and the dynamic stiffness of the mount and the vibration reduction performance of the mount were determined. It was shown that the addition of active control can reduce the effective dynamic stiffness of the mount by over a factor of 100 across the controlled frequency bandwidth. Furthermore, by appropriately applying the control force the dynamic stiffness of the mount can be driven toward zero at one or several frequencies. Transmitted vibration was reduced by over 20 dB relative to a passive mount and over 30 dB relative to a hard-mounted configuration.

Leo and Inman [66] discussed a quadratic programming algorithm for studying the tradeoffs of active-passive vibration isolation systems. The novelty of this technique is that the optimal control problem is posed as a quadratic optimization with linear constraints. The optimal active-passive isolation system was compared directly with a purely passive approach to determine the performance benefit of the active-passive design. Numerical studies showed that the performance advantage gained by the active system varied significantly with the energy content of the input. For the disturbance cases studied, the optimal control technique showed significant advantages over passive systems when the input energy shows a large increase near the break frequency of the isolation system.

Miller and Ahmadian [67] discussed the potential performance improvements that can be realized by adding electromagnetic actuators in parallel with traditional elastomeric or fluid mounts. Also discussed was the possibility of using piezoelectric or magnetostrictive materials to produce more efficient actuators. It was suggested that adaptive control algorithms could be very effective for controlling these hybrid mounts. It was also suggested that benefits of this technology could include improved vibration isolation and noise attenuation, higher static stiffness, and adaptable dynamic stiffness.

2.6 Power Scavenging

The subject of scavenging environmental energy to use for powering various devices has long been a scientific curiosity. Many types of energy have been harvested with varying degrees of success. Recent interest in power scavenging has led to an increase in research in this area. The following represents a summary of power scavenging literature to date.

2.6.1 Scavenging Footfall Energy

Increased interest in powering electrical devices, such as communication equipment for soldiers in the field, has led to several unique concepts for scavenging, storing and ultimately using this energy. All of these concepts are based on scavenging footfall energy. The following is a summary of the current literature on scavenged footfall energy.

Kymissis, Kendall, Paradiso and Gershenfeld [68] examined three different devices that can be built into a shoe to generate electrical power parasitically from walking. The three devices considered were a unimorph strip made from a piezoelectric composite material, a stave made from a multilayer laminate of PVDF foil, and a shoe-mounted rotary magnetic generator. It was shown that the rotary generator produces two orders of magnitude more power than either of the other generators, but was large and could not be incorporated inside the shoe. As an example of a potential application a circuit that periodically broadcasts a digital RFID as the wearer walks was designed around the three generators. It was shown that all three generators were capable of producing enough power to supply the circuitry.

Shenk's thesis [69] demonstrated the feasibility of generating and storing electric energy from the available mechanical energy in heel strikes. The generator considered

consisted of two Face International THUNDER™ unimorph piezoceramic transducers connected in parallel and mounted on opposite sides of a Be-Cu backplate which was then inserted into a sport sneaker. The resulting voltage was then converted into a useful form using high-frequency switching techniques. Much of the paper discusses this power conditioning circuitry and its evaluation.

2.6.2 Scavenging Vibration Energy

This section discusses the relevant literature whose subject is the scavenging of ambient vibration energy.

Amirtharajah and Chandrakasan [70] explored the feasibility of self-powering a DSP-based FIR filter, as well as a switching DC/DC converter, using converted ambient vibration energy. The generator consisted of a mass-spring system with a coil attached to the moving mass. The mass was attached to a spring and the spring was in turn attached to a rigid housing that could be subjected to external vibrations. Also encased in the housing was a permanent magnet that supplied the necessary magnetic field. A voltage was induced in the moving coil in accordance with Faraday's law. The excitation source considered was human walking. The voltage produced by the generator was stepped up using a transformer, rectified and used to power the load circuitry. It was shown that 400 μW of power could be generated which was enough to power the load circuitry entirely from ambient vibration energy. It was suggested that optimization of the generator's mechanical and electrical parameters could eliminate the need for a transformer.

Amirtharajah, Meninger, Mur-Miranda, Chandrakasan and Lang [71] discussed the use of a MEMS transducer to convert mechanical vibration into electrical energy for use in DSP-based sensor applications. The transducer consisted of a moving mass that had been etched with fingers which fit between fingers on a fixed comb. As the mass oscillates, these fingers slide past one another creating a variable area capacitance. The

resulting charge is scavenged to power an ultra-low-power DSP. It was shown that the transducer is capable of producing 8.66 μW of power.

Meninger, Mur-Miranda, Amirtharajah, Chandrakasan and Lang [72] proposed a system to convert ambient mechanical vibration energy into electrical energy. This system could be used to power an autonomous low-power electronic systems. Through the use of a variable capacitor that was designed with MEMS technology, the energy was transduced. A low power controller was fabricated, and it directed energy conversion and supplied power to the load. The controller consisted of a power electronics subsystem, which was responsible for exciting the transducer, and was optimized to minimize losses. A digital control core generated the timing pulses that drove the gates in the power electronics subsystem. A second capacitor of constant value was added in parallel to the MEMS device, and it was determined that the mechanical energy produced moved the plates apart and caused the voltage across the capacitor combination to reach a maximum. Thus the energy harvesting was performed. Based on predicted values of capacitance from the MEMS transducer, approximately 8μW was expected to be available for use by the load.

Umeda, Nakamura and Ueha [73] explored the transformation of mechanical impact energy to electrical energy using a piezoelectric generator consisting of an edge supported bronze disk to which a layer of piezoceramic material had been bonded. The excitation is provided by the impact of a free falling steel ball on the disk. Several interesting results were discussed. 1) It was determined that as the initial potential energy of the ball is increased, the maximum efficiency is decreased. 2) A large part of the energy is dissipated as the kinetic energy of the rebounding steel ball. 3) If the steel ball is allowed to stick to the piezogenerator and oscillate with it after impact an efficiency of greater than 50% can be achieved.

Umeda, Nakamura, K. and Ueha [74] investigated the conversion of mechanical impact energy to electrical energy using the impact of a steel ball on a piezoelectric vibrator. The AC output form the piezogenerator is rectified using a bridge rectifier and

stored in various batteries and capacitors. It was shown that the efficiency of the generation and storage is greater with a bridge rectifier as opposed to a single rectifier. Efficiencies of up to 35% were observer which is over three times the efficiency of a solar cell. It was concluded that this method of energy conversion and storage could be used to charge a practical battery or a large capacitor.

Williams and Yates [75] proposed a device, which generated electricity from mechanical energy when embedded in a vibrating environment. For their evaluation, an electromagnetic transducer was chosen. A harmonic analysis of the generator was performed in order to evaluate the viability of the device and optimize the design. It was determined from the analysis that the amount of power generated was proportional to the cube of the vibration frequency. This illustrated that the generator was likely to perform poorly at low frequencies. It was also determined that a low damping factor was required to maximize power generation, and therefore the design must allow for large deflections of the mass. For a typical device the predicted power generation was 1μW at an excitation frequency of 70 Hz, and 0.1mW at 330 Hz, (assuming a deflection of 50μm). Finally, it was determined that the choice of transducer had no direct effect on the amount of power generated.

2.6.3 Other Power Scavenging Applications

The following represents power scavenging literature that did not fit into the above categories, but was relevant nonetheless.

Choi and Cheong [54] discussed the development and testing of a suspension system consisting of an ER damper powered by a generator system consisting of a rack and pinion gear to transform the linear motion of the damper into rotary motion which was then amplified through additional gearing. The rotary motion wass then used to drive a generator and the resulting energy is stored in a battery to power the damper and control circuitry. It was shown that this fairly complex system could generate enough

power to operate the ER damper-based suspension. Furthermore, it was shown that acceptable vibration isolation could be achieved in terms of displacement transmissibility up to 2 Hz when utilized in a quarter car model.

Clark and Ramsey [76] conducted a design study that investigated the feasibility of using piezoelectric materials in a power supply for an in vivo MEMS application. The 33- and 31- modes of operation for a piezoelectric generator were analyzed and compared, and it was determined that when using the 31- mode, or thin plate configuration, there existed a strong mechanical advantage in converting applied pressure to working stress. For very low-pressure sources the 31- mode had a greater advantage in energy conversion, which became important when attempting to implement this technology in a biological micro system application. A design study was used to investigate whether or not the 31- mode was well suited for the in vivo environment, and it was carried out using a square thin plate driven by blood pressure. It was shown that ample power existed in the body from various sources to meet the requirements of their investigation, and additional calculations illustrated the feasibility of providing intermittent power instead of continuous power.

Fry, Holcomb, Munro, Oakes and Maston [77] provided a report that focused on advances in portable electric power sources made within the last two years, as well as assessing emerging PEPS technologies. Light weight, high power capacity, high reliability PEPS technology was emphasized in this report. It began by outlining the power source requirements that must be met in order for any new technology to be approved for use by Special Operations Forces. Potential power sources such as batteries, thin films, fuel cells, ultracapacitors, thermophotovoltaics, thermoelectric generators, various types of mechanical power sources, solar power, alkali metal to electric converters, and “exotic” portable power sources were all discussed. Power source standards were presented in order to address different concerns such as electrical and physical properties, environmental qualifications, maintenance, handling and disposal. Various tables were used to summarize the overall results of their assessments

of the power sources for use by SOCOM, and provided a comparison of portable power source technologies.

Hausler and Stein [78] proposed an implantable physiological power supply using PVDF films. Based on the concept that the energy expended for respiration could be converted into electric power, Hausler, et al, used the relative motion of the ribs to periodically stretch a converter. They designed a miniaturized prototype and conducted an animal experiment. A converter was fixed to the ribs of a dog and spontaneous breathing led to a peak voltage of 18V, which corresponded to a power of about 17μW. This power was insufficient for use as an implanted power supply, but optimization of the PVDF film properties, as well as more suitable converter attachment at the ribs, could make it possible to develop power converters with an electric power output of 1mW, yielding a mechanical power load of 20mW.

Starner [79] explored scavenging power from the human body to power wearable computing devices. The following potential sources of energy are discussed: Body heat, breath, blood pressure, upper limb motion, walking and finger motion. It was shown that the greatest amount of power derived from body-driven sources is footfall energy. It was shown that 5-8 W of power could be recovered by walking at a brisk pace.

2.7 Summary

Of all the work reviewed in the literature above, none considered the use of MR dampers in shipboard isolation systems. Furthermore, none of the papers discussed the use of MR dampers or air springs in combined shock and vibration isolation systems. Surprisingly no papers were found at all that specifically discussed the design of combined shock and vibration isolation systems.

In terms of power scavenging several papers were devoted to the scavenging of vibration energy, but none looked at the scavenging of ambient shipboard vibration

energy. Also, none of the papers looked at using scavenged energy to power MR dampers. Based on the results of the literature review it is clear that the subject shock and vibration isolation system and the associated power scavenging system has several novel features. Further strengthening the case for uniqueness of this work is the fact that this isolation system has passed a rigorous patent search by a reputable patent attorney. The result of the search showed that the isolation system included several patentable features and a patent application was filed listing 56 claims. Some of the patents that were discovered during the patent search included several patents for MR and ER fluid devices and two patents for piezoelectric energy generation devices [80-88]. This being the case much of this research has been previously unexplored and it follows that this work contributes to furthering the body of knowledge in the subject areas of combined shock and vibration isolation and self-powered, semiactive isolation systems.

Chapter 3

Shock and Vibration Isolation Theory

3.1 Vibration Isolation Theory

Shipboard vibration isolation can be broken down in terms of two distinct design goals, (1) isolating a piece of equipment from a moving base and (2) isolating the point of attachment of the equipment (deck or ground) from a moving piece of equipment. In shipboard isolation this is typically referred to as vibration and acoustic isolation, respectively. These two systems are shown graphically in Figures 3.1a and 3.1b

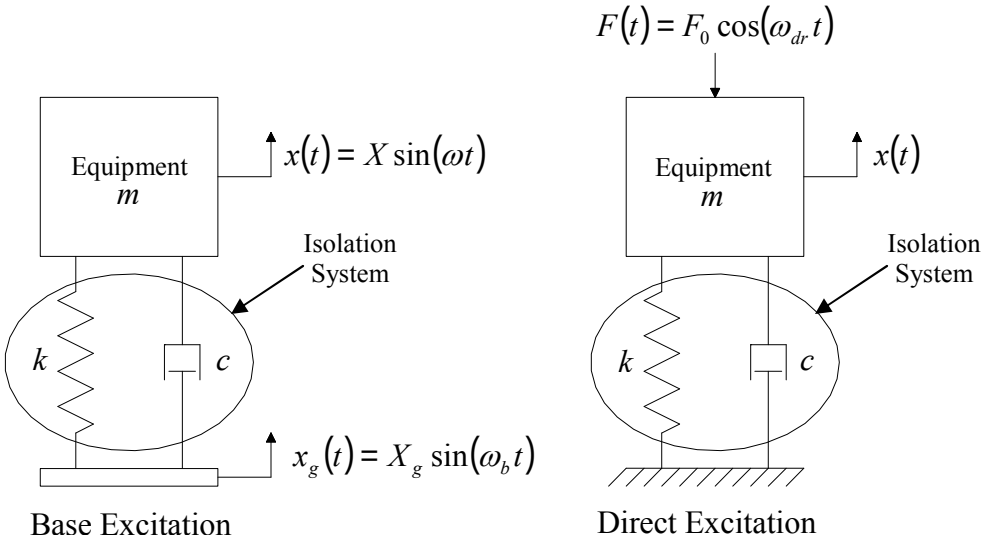

Figures 3.1a and 3.1b: Illustration of Two Typical Vibration Isolation Problems

Note that in Figure 3.1a the excitation source is the moving base and in Figure 3.1b the excitation source is the moving equipment. Consider first the direct excitation problem.

3.1.1 The Direct Excitation Problem

Applying Newton's Second Law to the system shown in Figure 3.1b leads to the equations of motion for the system,

$$m\ddot{x} + c\dot{x} + kx = F_0 \cos(\omega_{dr} t) \tag{3.1}$$

Dividing by mass m yields,

$$\ddot{x} + 2\zeta\omega\dot{x} + \omega^2 x = f_0 \cos(\omega_{dr} t) \tag{3.2}$$

where $\omega^2 = k/m$, $2\zeta\omega = c/m$ and $f_0 = F_0/m$. Now, the solution of Equation (3.2) will be the sum of the homogeneous solution and the particular solution, where the particular solution is the steady-state solution and the homogeneous solution is the transient solution. In this case we are interested in the particular solution as vibration isolation performance is typically measured in the steady-state. What happens during initial start-up transients is typically ignored. The exception is if the driving passes through the resonant frequency of the isolation system during start-up. This can lead to significant equipment responses, therefore, it is necessary to consider resonant conditions in any isolation system design. Here we will only consider the steady-state response and hence are only interested in the particular solution.

From a first course in differential equations it is known that the forced response of a damped system is a harmonic function of the same frequency as the driving force, but with a different amplitude and phase. Therefore, assume a particular solution of the form,

$$x_p(t) = A_0 \cos(\omega_{dr} t - \phi) \tag{3.3}$$

which can be written in the equivalent form,

$$x_p(t) = A_s \cos(\omega_{dr} t) + B_s \sin(\omega_{dr} t) \tag{3.4}$$

where the constants A_s and B_s satisfy,

$$A_0 = \sqrt{A_s^2 + B_s^2} \text{ and } \phi = \tan^{-1}\left(\frac{B_s}{A_s}\right) \tag{3.5}$$

Taking derivatives of the assumed form of the solution given by Equation (3.4) and substituting into Equation (3.2) gives,

$$\begin{aligned} &\left(-\omega_{dr}^2 A_s + 2\zeta\omega\omega_{dr} B_s + \omega^2 A_s - f_0\right)\cos(\omega_{dr} t) + \ldots \\ &\ldots + \left(-\omega_{dr}^2 B_s - 2\zeta\omega\omega_{dr} A_s + \omega^2 B_s\right)\sin(\omega_{dr} t) = 0 \end{aligned} \tag{3.6}$$

Now, Equation (3.6) must hold for all time. In particular, it must hold for $t = 2\pi/\omega_{dr}$, therefore, the coefficient of $\cos(\omega_{dr} t)$ must vanish. A similar argument can be made for the coefficient of $\sin(\omega_{dr} t)$. Simultaneously satisfying both requirements leads to the following system of equations for the two undetermined coefficients,

$$\begin{aligned} A_s &= \frac{\left(\omega^2 - \omega_{dr}^2\right) f_0}{\left(\omega^2 - \omega_{dr}^2\right)^2 + \left(2\zeta\omega\omega_{dr}\right)^2} \\ B_s &= \frac{2\zeta\omega\omega_{dr} f_0}{\left(\omega^2 - \omega_{dr}^2\right)^2 + \left(2\zeta\omega\omega_{dr}\right)^2} \end{aligned} \tag{3.7}$$

Substituting Equations (3.7) into Equation (3.5), and the result into Equation (3.4), leads to the particular solution,

$$x_p(t) = \underbrace{\frac{f_0}{\sqrt{\left(\omega^2 - \omega_{dr}^2\right)^2 + \left(2\zeta\omega\omega_{dr}\right)^2}}}_{A_0} \cos\left(\omega_{dr}t - \underbrace{\tan^{-1}\left(\frac{2\zeta\omega\omega_{dr}}{\omega^2 - \omega_{dr}^2}\right)}_{\phi}\right) \tag{3.8}$$

Obviously the total solution would also contain the homogeneous solution, but here it is omitted as was discussed previously.

Now, consider the magnitude of the particular solution,

$$A_0 = \frac{f_0}{\sqrt{\left(\omega^2 - \omega_{dr}^2\right)^2 + \left(2\zeta\omega\omega_{dr}\right)^2}} \tag{3.9}$$

Factoring out ω^2, dividing by F_0/m, and substituting $r = \omega_{dr}/\omega$, where is defined as the frequency ratio leads to,

$$\frac{A_0 k}{F_0} = \frac{1}{\sqrt{\left(1 - r^2\right)^2 + \left(2\zeta r\right)^2}} \tag{3.10}$$

Equation (3.10) represents the ratio of the peak force transmitted to the base $A_0 k$ to the magnitude of the applied force F_0. Figure 3.2 is a plot of Equation (3.10). This plot represents graphically the force transmissibility from the driven mass to the base as a function of the frequency ratio for various damping values. It can be seen that the maximum transmissibility occurs when $\omega_{dr} = \omega$, or resonance. It should be noted that true resonance does not exactly occur when $\omega_{dr} = \omega$, but this is the commonly accepted definition of resonance. By looking at Figure 3.2 it is clear that defining resonance to occur at $\omega_{dr} = \omega$ is sufficient for most design purposes. It should also be noted that the force transmissibility decreases as damping increases for all values of .

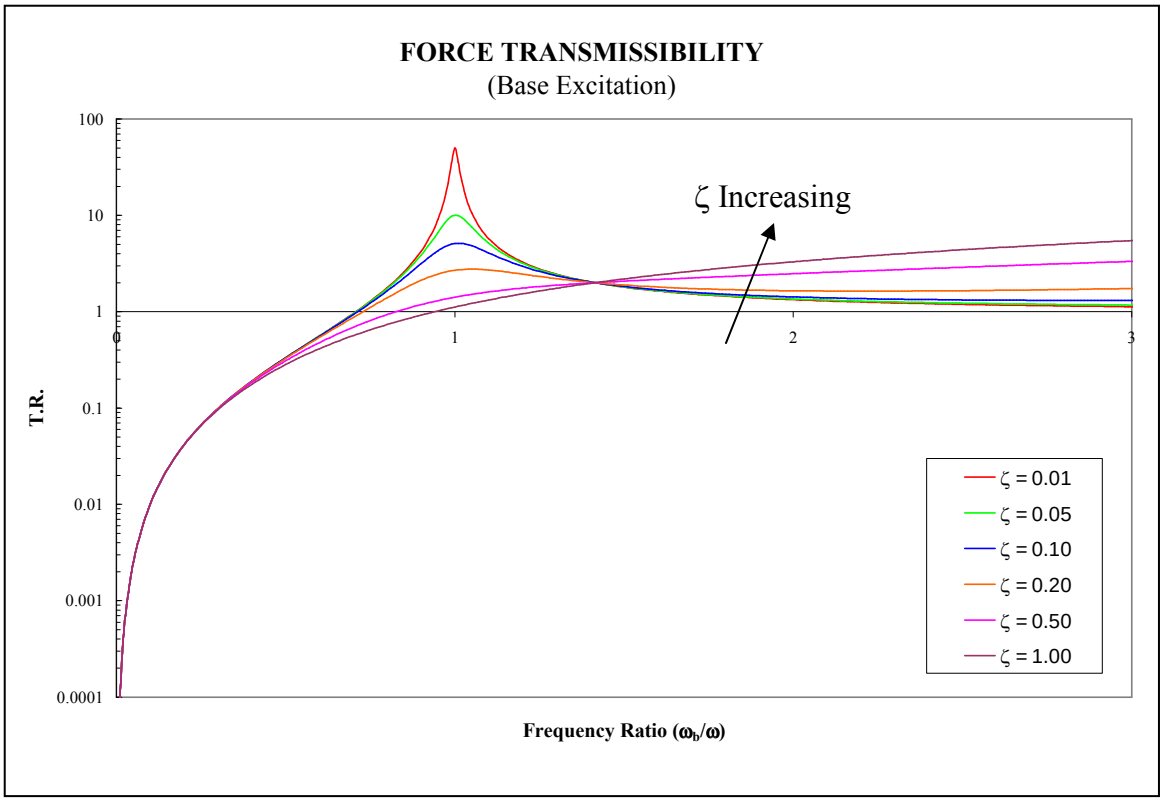

Figure 3.2: Force Transmissibility (Direct Excitation)

3.1.2 The Base Excitation Problem

Applying Newton's Second Law to the system shown in Figure 3.1a leads to the equations of motion for the system,

$$m\ddot{x} + c\left(\dot{x} - \dot{x}_g\right) + k\left(x - x_g\right) = 0 \tag{3.11}$$

Substituting the assumed form for the base excitation $x_g(t) = X_g \sin(\omega_b t)$ into Equation (3.11) yields,

$$m\ddot{x} + c\dot{x} + kx = cX_g\omega_b \cos(\omega_b t) + kX_g \sin(\omega_b t) \tag{3.12}$$

Dividing Equation (3.12) by m and using the definitions of damping ratio and natural frequency defined in Section 3.1.1 leads to,

$$\ddot{x} + 2\zeta\omega\dot{x} + \omega^2 x = 2\zeta\omega\omega_b Y\cos(\omega_b t) + \omega^2 Y\sin(\omega_b t) \tag{3.13}$$

As explained in Section 3.1.1 the particular solution to Equation (3.13) is desired. The particular solution to Equation (3.13) consists of two parts, one for each harmonic input. The particular solution for the first harmonic input $2\zeta\omega\omega_b Y\cos(\omega_b t)$ follows from the method of undetermined coefficients as detailed in Section 3.1.1. The solution can be determined directly by substituting $2\zeta\omega\omega_b Y$ for f_0 in Equation (3.8). The result is,

$$x_p^{(1)} = \frac{2\zeta\omega\omega_b Y}{\sqrt{\left(\omega^2 - \omega_b^2\right)^2 + \left(2\zeta\omega\omega_b\right)^2}}\cos\left(\omega_b t - \tan^{-1}\left(\frac{2\zeta\omega\omega_b}{\omega^2 - \omega_b^2}\right)\right) \tag{3.14}$$

The particular solution for the second harmonic input $\omega^2 Y\sin(\omega_b t)$ can be determined by following the method of undetermined coefficients as detailed in Section 3.1.1. The result is,

$$x_p^{(2)} = \frac{\omega^2 Y}{\sqrt{\left(\omega^2 - \omega_b^2\right)^2 + \left(2\zeta\omega\omega_2\right)^2}}\sin\left(\omega_b t - \tan^{-1}\left(\frac{2\zeta\omega\omega_b}{\omega^2 - \omega_b^2}\right)\right) \tag{3.15}$$

By the principle of superposition the total particular solution is the sum of the two particular solutions given by Equations (3.14) and (3.15). Therefore, the total particular solution is,

$$\begin{aligned} x_p(t) &= x_p^{(1)} + x_p^{(2)} \\ &= \omega Y\left[\frac{\omega^2 + (2\zeta\omega)^2}{\left(\omega^2 - \omega_b^2\right)^2 + \left(2\zeta\omega\omega_b\right)^2}\right]^{1/2}\cos\left(\omega_b t - \tan^{-1}\left(\frac{2\zeta\omega\omega_b}{\omega^2 - \omega_b^2}\right) - \tan^{-1}\left(\frac{\omega}{2\zeta\omega_b}\right)\right) \end{aligned} \tag{3.16}$$

Defining the magnitude of the particular solution $x_p(t)$ by X and utilizing the definition of the frequency ratio $r = \omega_b/\omega$ yields,

$$X = Y\left[\frac{1+(2\zeta\omega)^2}{(1-r^2)^2+(2\zeta r)^2}\right]^{1/2} \tag{3.17}$$

Dividing Equation (3.17) by Y gives,

$$\frac{X}{Y} = \left[\frac{1+(2\zeta\omega)^2}{(1-r^2)^2+(2\zeta r)^2}\right]^{1/2} \tag{3.18}$$

Equation (3.18) represents the ratio of the maximum response magnitude to the input displacement magnitude, or the displacement transmissibility. Equation (3.18) is plotted in Figure 3.3. From the figure it can be seen that for frequency ratios less than $\sqrt{2}$ the motion of the isolated mass is greater in amplitude that the motion of the base. However, for frequency ratios greater than $\sqrt{2}$ the amplitude of the motion of the isolated mass is less than that of the base. Therefore, if isolation in terms of diminished motion of the isolated mass is the design goal, then it is desirable for the isolation system to have a natural frequency ω that results in a frequency ratio greater than $\sqrt{2}$. It should also be noted that the effectiveness of the isolation system in terms of displacement transmissibility is diminished as the damping ratio increases. Therefore, if minimizing displacement transmissibility is the design goal then the isolation system should be lightly damped.

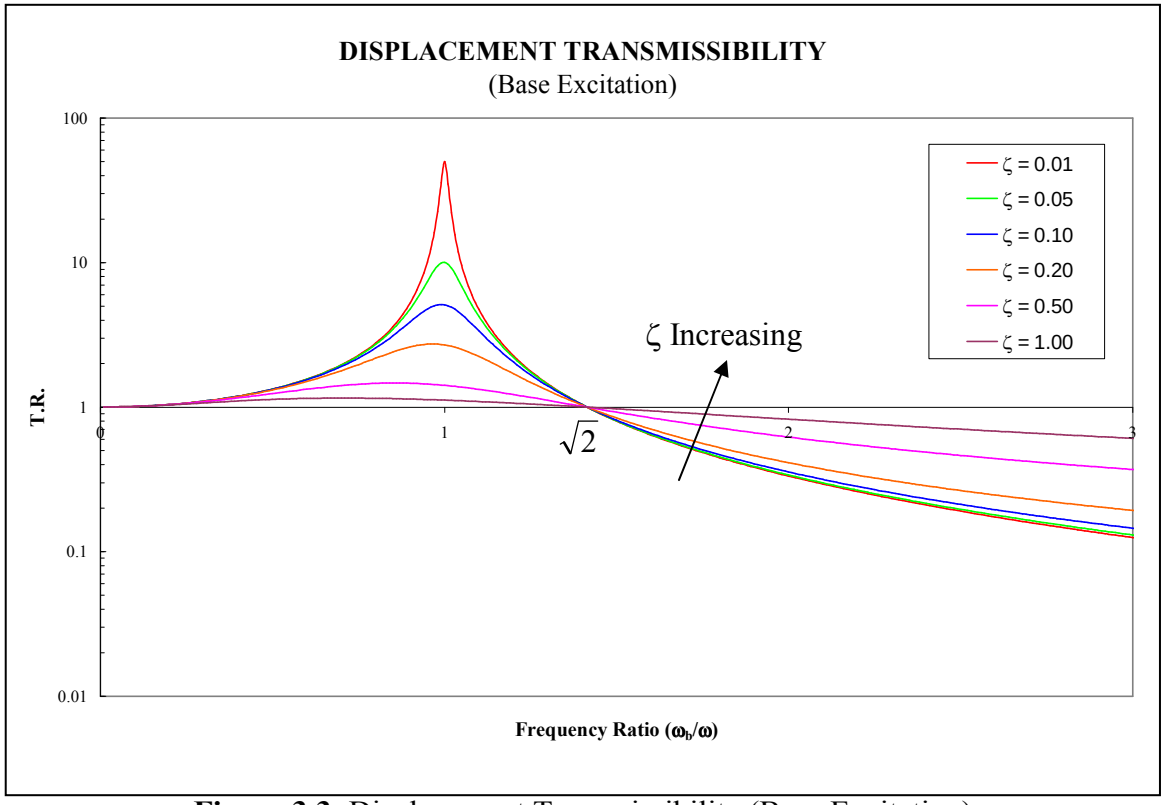

Figure 3.3: Displacement Transmissibility (Base Excitation)

Another quantity of interest is the force transmitted from the motion of the base to the isolated mass. The transmitted force is the sum of the spring force and the damper force, or

$$F_T(t) = k(x - x_b) + c(\dot{x} - \dot{x}_b) \tag{3.19}$$

This force must be equivalent to the inertial force of the mass, or

$$F_T(t) = k(x - x_b) + c(\dot{x} - \dot{x}_b) = -m\ddot{x}(t) \tag{3.20}$$

Therefore, the equation describing the transmitted force can be obtained by differentiating Equation (3.16) twice and substituting the result in Equation (3.20). The result is,

$$F_T(t) = m\omega\omega_b^2 Y\left[\frac{\omega^2 + (2\zeta\omega_b)^2}{(\omega^2 - \omega_b^2)^2 + (2\zeta\omega\omega_b)^2}\right]^{1/2} \cos\left(\omega_b t - \tan^{-1}\left(\frac{2\zeta\omega\omega_b}{\omega^2 - \omega_b^2}\right) - \tan^{-1}\left(\frac{\omega}{2\zeta\omega_b}\right)\right) \tag{3.21}$$

Therefore, the magnitude of the transmitted force is,

$$F_T = m\omega\omega_b^2 Y\left[\frac{\omega^2 + (2\zeta\omega_b)^2}{(\omega^2 - \omega_b^2)^2 + (2\zeta\omega\omega_b)^2}\right]^{1/2} \tag{3.22}$$

Substituting the definition for the frequency ratio $r = \omega_b/\omega$ into Equation (3.22) gives,

$$F_T = kYr^2\left[\frac{1 + (2\zeta r)^2}{(1 - r^2)^2 + (2\zeta r)^2}\right]^{1/2} \tag{3.23}$$

Dividing Equation (3.23) by kY results in the force transmissibility ratio,

$$\frac{F_T}{kY} = r^2\left[\frac{1 + (2\zeta r)^2}{(1 - r^2)^2 + (2\zeta r)^2}\right]^{1/2} \tag{3.24}$$

This equation represents the ratio of the magnitude of the force transmitted to the isolated mass to the magnitude of the force applied to the isolation system due to the motion of the base. Figure 3.4 is a plot of Equation (3.24). Note that unlike the displacement transmissibility, the force transmissibility does not necessarily decrease for all $r > \sqrt{2}$. In fact as damping increases the transmitted force can increase significantly for $r > \sqrt{2}$.

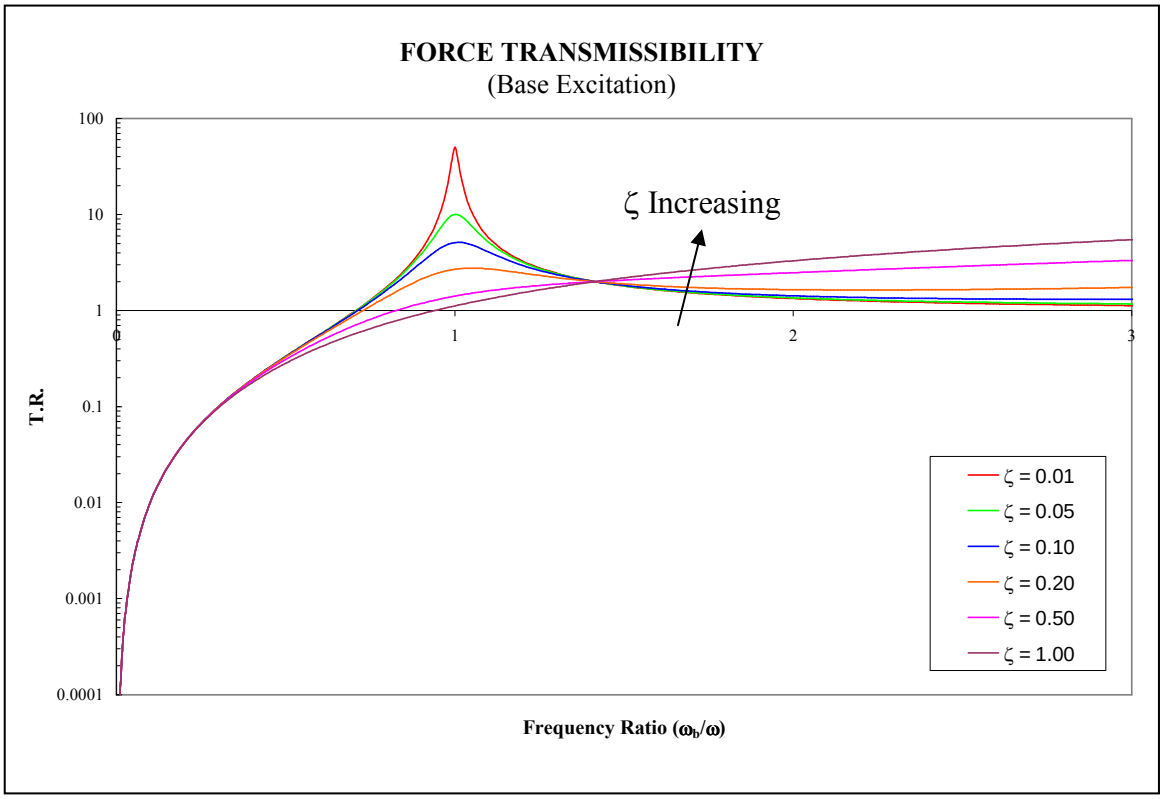

Figure 3.4: Force Transmissibility (Base Excitation)

3.2 Shock Isolation Theory

If the input to the base in the base excitation problem is a shock as opposed to a harmonic input, the resulting response is quite different. Shock inputs tend to excite all resonances in a system simultaneously, particularly the resonance of the isolation system itself. Thus a shipboard shock isolation system must be designed to dissipate considerable amounts of energy in a minimal amount of time. This is typically accomplished though some form of damping mechanism. Therefore a good shock isolator typically is heavily damped. To investigate the effect of increased damping on a shock isolation system consider the base excitation problem with the input being a half sinusoid of the form,

$$x_g(t) = \begin{cases} Y \sin \omega_p t & 0 \le t \le t_1 = \dfrac{\pi}{\omega_p} \\ 0 & t > t_1 = \dfrac{\pi}{\omega_p} \end{cases} \tag{3.25}$$

Figure 3.5 is as plot of the response of a 2.27 Hz isolator to the base excitation described in Equation (3.25).

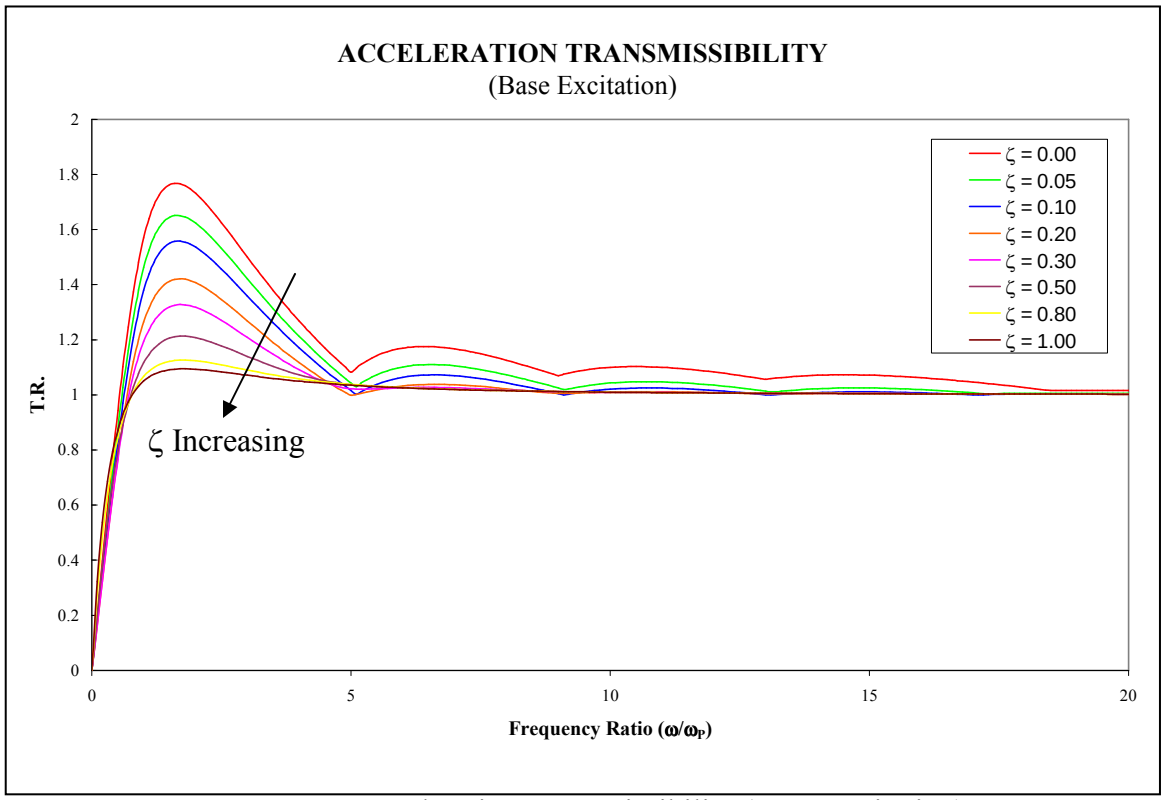

Figure 3.5: Acceleration Transmissibility (Base Excitation)

From Figure 3.5 it can be seen that in terms of shock isolation performance it is desirable for the isolation system to be heavily damped.

3.3 Combined Shock and Vibration Isolation

A common misconception is that a good shock isolation system must be mechanically "stiff". In reality "soft" isolation systems, such as air springs perform very well as shock isolators. A soft system tends to behave as a mechanical low pass filter and any high frequency input, such as typical ship-shock input, tend to be mitigated when passing through a low frequency device. Very little of this high frequency energy passes through to the isolated mass. However, the problem with a low frequency device is that shock inputs tend to excite the resonance of the isolator. Being a low frequency device this tends to result in significant deflections that are often unacceptable due to rattle space requirements.

By looking at Figures 3.3 and 3.4 it can be seen that increasing damping is detrimental to both the force and displacement transmissibility under vibration inputs. However, as was shown in Figure 3.5 large amounts of damping are required in a shock isolation system. This is the classic trade-off in shock and vibration isolation system design. A good compromise is to use a controllable damper that provides light damping in vibration isolation mode, but can be turned on during a shock event to provide the large amounts of damping necessary for controlling the effect of the shock input.

Chapter 4

Ship Shock Analysis and Testing

4.1 Ship Shock Inputs

A ship can be subjected to many different types of shock inputs such as wave slap, impact, weapons air blast, etc. In this dissertation it is assumed that the shock input to the ship is due to a near-miss underwater weapons explosion. Typically this is the most damaging input to a ship and is the input most often considered in ship design. A weapon exploding underwater produces a gas bubble that initially expands rapidly and simultaneously an initial transient pressure wave propagates outward. As the bubble is forming it is simultaneously being carried toward to water surface by buoyant forces. At some point the internal pressure in the bubble cannot support the weight of the surrounding water and the bubble collapses. The implosion of the bubble causes a second pressure wave to propagate (the so-called "Bubble Pulse") and the bubble expands again. This process is repeated until the bubble breaks the surface of the water. The bubble development is shown graphically in Figure 4.1.

Figure 4.1: UNDEX Bubble Development

The propagating pressure wave is the destructive force in these near-miss explosive events. In terms of destructive potential the initial transient is the most damaging to a ship. However, the pressure wave developed by the first bubble collapse can be significant in terms of damage potential as well.

The pressure waves produced by the underwater explosion then propagate through the water and eventually impinge upon the ship's hull. This pressure wave then excites the ship's structure. Equipment that is mounted near the hull experiences a shock that is similar to the hull motion. A typical hull-level motion due to an underwater explosion is shown in Figure 4.2.

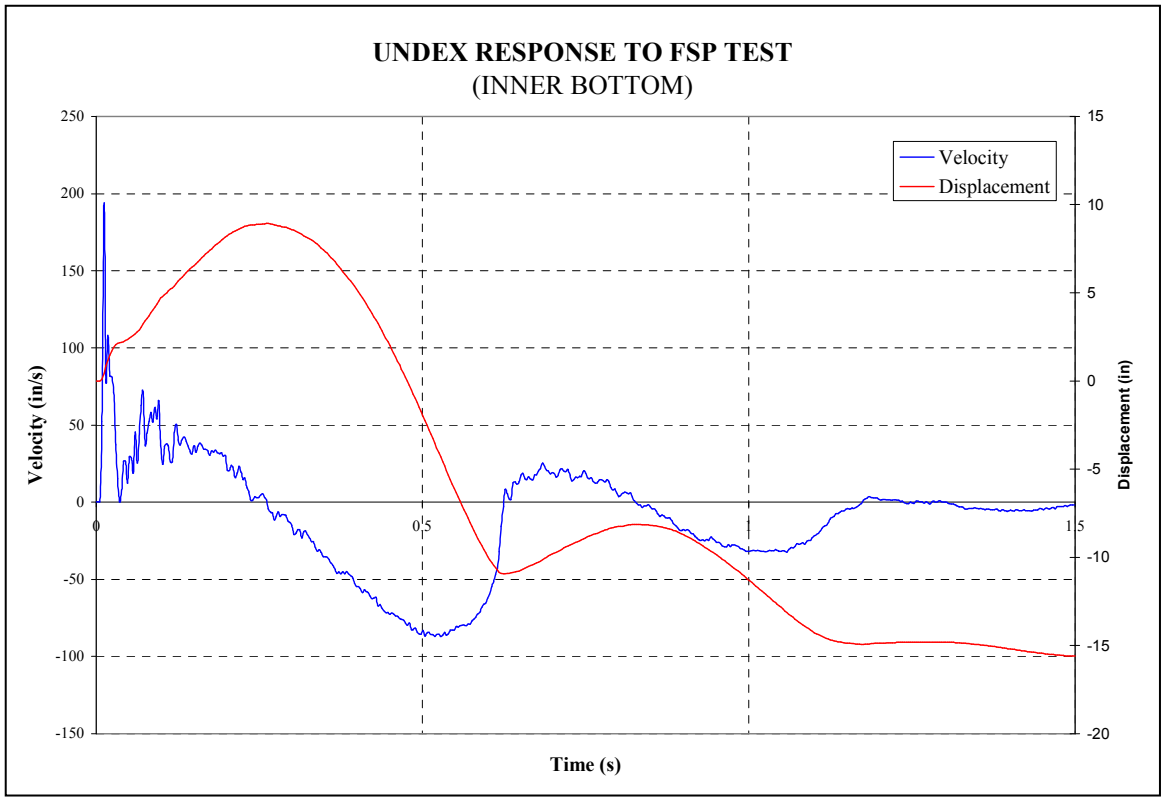

Figure 4.2: Typical Hull-Level Response to an UNDEX Event

Note that the input tends to contain fairly high frequencies and that the majority of the energy is contained in the early time. As the energy travels through the ship's structure it is dissipated through structural damping and other means. In addition its character is modified by the excited structure. For example, a deck excited by the

propagating shock wave will oscillate at its fundamental frequency. Figure 4.3 is a plot of a typical deck-level motion.

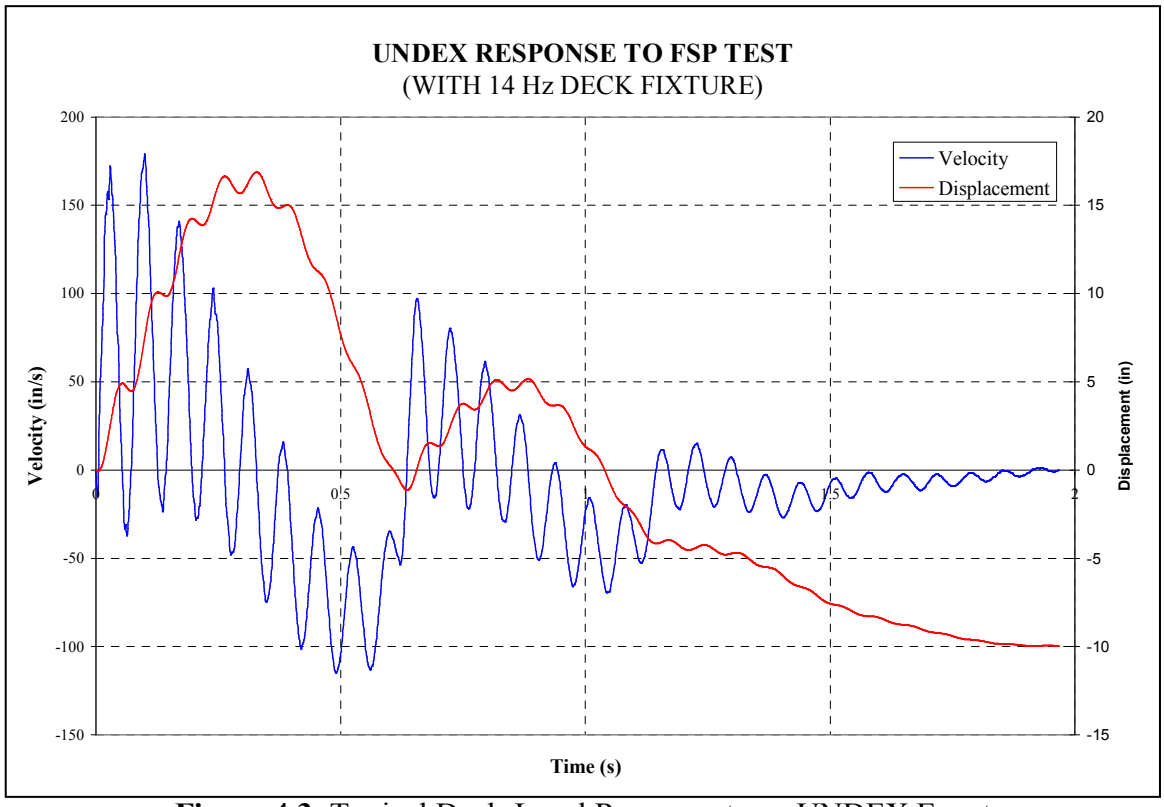

Figure 4.3: Typical Deck-Level Response to an UNDEX Event

Note that the amplitude of the motion has been reduced due to the dissipation of the energy as the wave propagates through the ships structure. Also note the predominant frequency content at the deck-level occurs at the fundamental frequency of the deck, in this case 14 Hz.

4.2 Navy Shock Test Machines

Due to the danger and difficulty of shock testing a ship with underwater explosives, several machines have been developed over the years to simulate an input due

to an UNDEX event. Figures 4.4 through 4.6 depict the currently accepted Navy shock test machines.

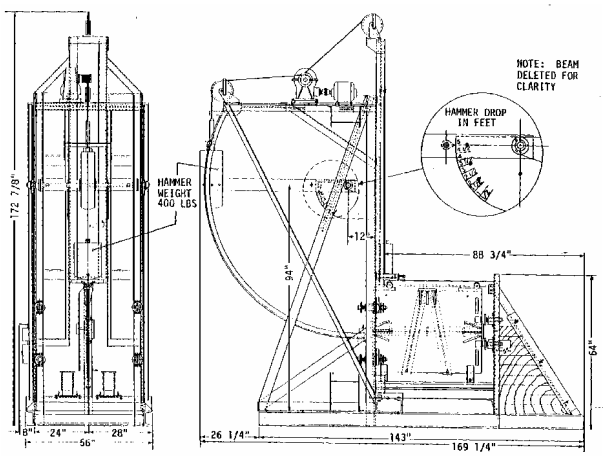

Figure 4.4: Lightweight Shock Machine

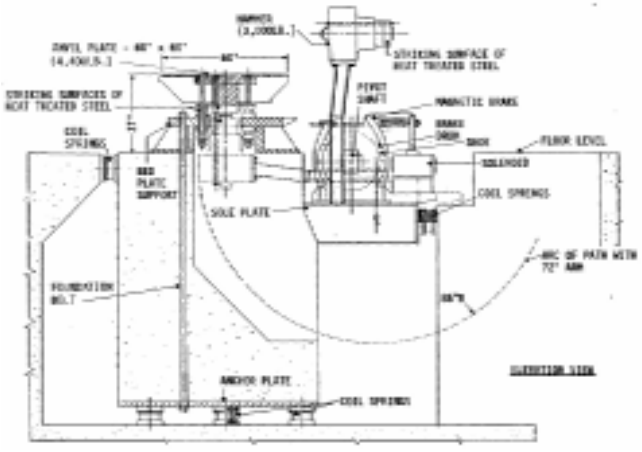

Figure 4.5: Medium Weight Shock Test Machine

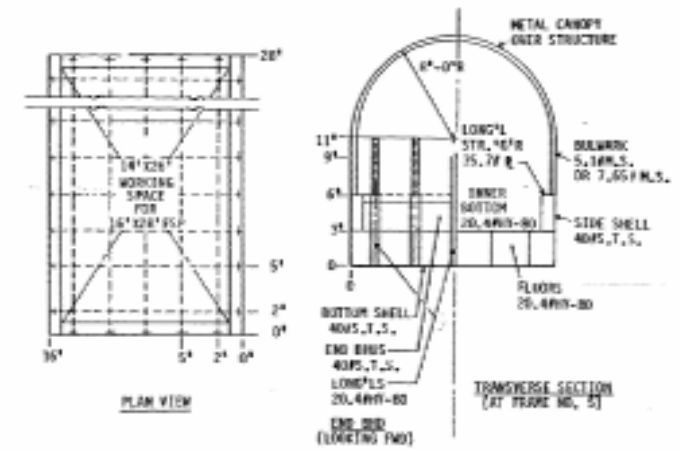

Figure 4.6: Floating Shock Platform

The decision to use one machine or the other is based on the weight of the equipment to be tested. The Lightweight Shock Machine, shown in Figure 4.4 is used for test articles up to 350 lbs. The Medium Weight Shock Machine, shown in Figure 4.5, is used for test articles up to 7,400 lbs. The Floating Shock Platform, shown in Figure 4.6, is used for test articles of up to 60,000 lbs. The Lightweight and Medium Weight Shock Machine are impact machines and the excitation to the test article is provided by a hammer impacting an anvil. With the Floating Shock Platform the excitation is provided by a high explosive charge placed underwater at various stand-off distances from the FSP. Figure 4.7 shows an FSP undergoing a test. Note that a typical test only involves one charge and that Figure 4.7 represents a rare double shot.

Figure 4.7: FSP During an UNDEX Test (Double Shot)

The FSP is essentially a floating barge to which test articles can be attached. The FSP arguably provides a more accurate representation of what happens on an actual ship during an UNDEX event. To simulate a hull-mounted condition test articles can be mounted directly to inner bottom of the hull. To simulate a deck mounted condition Deck Simulator Fixtures (DSF) can be installed in the FSP to simulate deck of various frequencies.